Proton Transfer in Malonaldehyde: An Ab Initio Projector Augmented Wave Molecular Dynamics Study**

Katharina Wolf, Werner Mikenda,* Ernst Nusterer, Karlheinz Schwarz, and Claudia Ulbricht

Abstract: Proton transfer in malonaldehyde was studied by molecular dynamics simulations with the projector augmented wave (PAW) method, which combines classical dynamics with ab initio quantum mechanical forces. The PAW trajectories were calculated for several temperatures between 1 and 600 K, for evolution time periods up to 20 ps, and with a constant time interval of 0.12 fs. At elevated temperatures proton transfer is not associated with a well-defined C_{2v}-symmetric transition state, but takes place in widely differing geometric situations. Although a short O – O distance favors proton transfer, it is neither a sufficient nor a necessary condition. Analysis of the data by a discriminant method and with a neural network yielded several relevant molecular parameters, and the resulting discrimination functions predicted the occurrence of proton transfer with an accuracy greater than 95%. The energetics of the proton motion was modeled by calculating time evolutions of the potential energy along a properly chosen reaction coordinate within a heavy–light–heavy atom approximation. At any instant the proton motion is governed by this potential, but while the proton moves, the potential also changes due to the dynamics of the molecule. Three extremes can be distinguished: i) Normal periods, in which the proton is trapped at one oxygen atom. The proton is stationary within an approximately constant, strongly asymmetric potential; the frequency of about 2850 cm^{-1} is close to the experimentally observed ν(OH) frequency. ii) Statistical isolated proton-transfer transitions, in which the proton rapidly moves from one oxygen atom to the other. The process starts and ends with strongly asymmetric potentials, but passes through (nearly) symmetric double- or single-minimum potentials. iii) Proton-shuttling periods, which include several consecutive nonstatistical transitions. These are not true proton transfers. The proton is (quasi)-stationary within a (nearly) symmetric single-minimum potential, which remains approximately constant for a longer time period; the motion corresponds to a ν(OH) vibration with a frequency of about 2000 cm^{-1}.

Keywords: ab initio calculations · molecular dynamics · projector augmented wave method · tautomerism

Introduction

Intramolecular hydrogen bonding and proton transfer in malonaldehyde has been studied extensively in the last two decades both by experiment[2–6] and by theory.[7–15] According to microwave investigations,[3] in the vapor phase malonaldehyde exists in a planar, intramolecularly hydrogen-bonded *cis*-enol form with two symmetrically equivalent tautomeric equilibrium configurations (Figure 1), between which proton transfer takes place. From the observed ground state tunneling splitting $\Delta E_{01} = 21.6$ cm^{-1} a tunneling rate of 1.2×10^{-12} s^{-1} and a tunneling barrier of approximately 28 $kJ\,mol^{-1}$ have been estimated.[3] Vapor-phase[4] and matrix-isolation[5] IR spectra are in agreement with the structure determined by microwave spectroscopy, and a more recent high-resolution

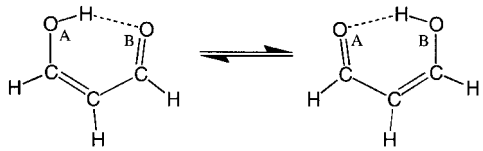

Figure 1. The two tautomeric equilibrium configurations of malonaldehyde (according to microwave data[3]).

[*] Prof. Dr. W. Mikenda, K. Wolf
Institute of Organic Chemistry
University of Vienna
Währingerstrasse 38, A-1090 Vienna (Austria)
Fax: (+43) 1-31367-2280
E-mail: werner.mikenda@univie.ac.at
E. Nusterer, K. Schwarz
Institute of Technical Electrochemistry
Vienna University of Technology (Austria)
C. Ulbricht
Austrian Research Institute for Artificial Intelligence (Austria)

[**] Presented in part at the XIIth Conference Workshop Horizons in Hydrogen Bond Research, Niederöblarn, Austria, 1997.[1]

0947-6539/98/0408-1418 $ 17.50+.50/0

far-IR study[6] confirms the value of the ground state tunneling splitting determined by microwave spectroscopy. In agreement with the experimental findings, higher level ab initio quantum chemical geometry optimizations[7, 8] also predict the asymmetric, intramolecularly hydrogen-bonded *cis*-enol form of malonaldehyde to be the most stable configuration. For the proton-transfer process point-to-point calculations yield a C_{2v}-symmetric transition state. The barrier height is highly sensitive to the level of theory. Recently a value of 14 kJ mol^{-1} has been obtained at the MP2/6-31 + G(3df,2p) level of theory,[8] which is about half of the above experimental estimate, but it can be expected that enlargement of the basis set and/or the inclusion of higher order correlation interaction terms will lead to a further decrease in the barrier.

Since malonaldehyde is the smallest molecule capable of intramolecular proton transfer, it has also been the subject of a number of dynamics studies and, in particular, it has often served as a prototype and test molecule for models of proton-tunneling processes. Sophisticated methods have been developed to reproduce the experimental tunneling splitting,[9–15] and significant progress has been achieved by two-[12] and multidimensional[13–15] approaches. In a recent study,[15] based on the Makri – Miller model,[14] the potential energy surface was calculated from the experimental data of a complete vibrational force field, and a tunneling barrier height of 42 kJ mol^{-1} was assumed. This study yielded a ground state tunneling splitting of 21.8 cm^{-1}, in excellent agreement with experiment, despite the fact that accurate ab initio calculations suggest that the assumed barrier height is much too high. Besides studies on proton tunneling, other kinetic or dynamic studies of intramolecular proton transfer in malonaldehyde by well-established standard methods such as transition state theory and its refinements or classical and semiclassical trajectory simulation seem to be scarce.[16, 17] With regard to the present work we note that Hutchinson[17] performed a classical trajectory simulation at energies above the transfer barrier, which was based on a simplified model with two degrees of freedom (O – H stretching and C-O-H bending motions with an otherwise fixed geometry). He distinguished between three categories of reactive trajectories: those that cross the transition state and become trapped or recross immediately, those in which the proton oscillates quasiperiodically between the two oxygen atoms, and those with chaotic proton motion.

In the course of our experimental and theoretical studies on intramolecular hydrogen bonding[18] we performed ab initio molecular dynamics simulations of malonaldehyde with the projector augmented wave method (PAW),[19] which is based on the direct ab initio molecular dynamics approach of Car and Parrinello (CPMD),[20] in which classical dynamics are combined with ab initio quantum mechanical forces. The main feature of the CPMD approach is that the potential energy surface (PES) is neither fitted to experimental data nor constructed on the basis of arbitrary assumptions; the all-electron wave function is available for any time step although the whole PES is not known analytically; the corresponding forces are calculated directly from first principles by accurate density functional theory, whereas the dynamics of the electron wave functions are introduced by using a fictitious Lagrangian to describe their motion. The atoms are propagated following classical Newtonian equations of motion, whereas the forces acting on the nuclei are obtained by solving the electronic structure problem at each time step. The PAW method is the first all-electron method for CPMD; a sophisticated augmentation scheme is used to create the all-electron wave functions with the correct nodal structure. This augmentation makes PAW especially efficient for the study of systems that contain first-row elements or transition metals,[21] and recently the method has successfully been applied to problems in physics, chemistry, and biochemistry.[22] Since all nuclear motions are treated classically, PAW does not account

Abstract in German: *Zur Untersuchung des Protonentransfers in Malonaldehyd wurden ab initio Molekulardynamik-Simulationen mit Hilfe der Projector Augmented Wave Methode (PAW) durchgeführt. PAW-Trajektorien wurden bei einem konstanten Zeitintervall von 0.12 fs für Temperaturen zwischen 1 und 600 K über Zeitspannen von bis zu 20 ps berechnet. Bei endlichen Temperaturen erfolgt der Protonentransfer nicht über einen wohldefinierten C_{2v} symmetrischen Übergangszustand, sondern kann bei sehr unterschiedlichen geometrischen Bedingungen stattfinden. Ein kurzer R(OO)-Abstand begünstigt zwar den Protonentransfer, doch ist dies weder eine notwendige noch eine hinreichende Bedingung für den Prozeß. Eine Datenanalyse mittels Diskriminanzanalyse und mit einem neuronalen Netzwerk ergab mehrere weitere wichtige Molekül-Parameter und mit Hilfe der resultierenden Diskriminanzfunktionen konnte das Auftreten von Protonentransfer in 95 % der Fälle korrekt vorhergesagt werden. Die Energetik der Protonenbewegung wurde mit Hilfe von Modellrechnungen nachvollzogen. Dazu wurde die Zeitevolution der potentiellen Energie entlang einer geeigneten Reaktionskoordinate im Rahmen einer heavy-light-heavy Näherung berechnet. Zu jedem Zeitpunkt wird die Protonenbewegung durch dieses Potential determiniert, doch während sich das Proton bewegt, ändert sich, in Folge der Moleküldynamik, ständig auch dieses Potential. Drei extreme Situationen lassen sich unterscheiden: 1) normale Perioden, in denen das Proton an einen Sauerstoff gebunden bleibt und eine stationäre Bewegung in einem annähernd konstanten, stark asymmetrischen Potential ausführt (entsprechend einer ν(OH) Schwingung mit der Frequenz 2850 cm^{-1}, in ausgezeichneter Übereinstimmung mit dem experimentellen Wert); 2) statistische isolierte Protonentransferprozesse, bei denen sich das Proton rasch und stetig vom einen zum anderen Sauerstoff bewegt. Der Transfer startet und endet mit stark asymmetrischen Potentialen, verläuft jedoch über annähernd symmetrische Doppel- oder Singelminimumpotentiale; 3) proton-shuttling-Perioden, die mehrere aufeinanderfolgende, nicht-statistische Übergänge beinhalten. In diesen Fällen handelt es sich nicht um echte Protonentransferprozesse, sondern viel mehr um eine vorübergehende stationäre Protonenbewegung (entsprechend einer ν(OH) Schwingung mit einer Frequenz von etwa 2000 cm^{-1}) in einem annähernd symmetrischen Singelminimumpotential, das über längere Zeit annähernd konstant bleibt.*

for quantum effects such as proton tunneling or zero-point motion, unlike the above-mentioned tunneling studies on malonaldehyde. However, PAW yields full ab initio dynamics of the molecule on a picosecond time scale at finite temperatures and hence may provide another valuable viewpoint for understanding the proton-transfer process.

Here we report a PAW study of malonaldehyde, which to the best of our knowledge is the first parameter-free, finite-temperature molecular dynamics simulation of an intramolecular proton-transfer process. Results were extracted by means of time evolutions of several molecular parameters that characterize the hydrogen-bonded chelate ring. It is shown that it is reasonable to discriminate between two extreme cases of proton transfer: statistical isolated transitions and nonstatistical quasistationary shuttling transitions. We also deal with the question of systematic relationships between distinct molecular parameters and the occurrence of proton-transfer processes. Results were obtained both by a discriminant analysis and with the aid of a neural network. Finally, we show that the observed proton motion can be reasonably well understood in terms of the potential energy along an appropriately chosen proton-transfer reaction coordinate, which to a first approximation determines this motion, and which, due to the dynamics of the molecule, permanently changes while the proton moves.

Methods

The PAW molecular dynamics (MD) simulations were performed at temperatures between 1 K and 600 K for evolution time periods of 2 – 20 ps with a constant time-interval of $\Delta t = 5$ au (0.1209 fs); altogether our calculations cover about 600 000 single time steps. The temperature of the MD runs was controlled with the Nosè – Hoover thermostat.[23] The MD runs started with an arbitrary geometry and random forces and were equilibrated for about 5000 time steps to eliminate possible effects of the initial conditions. We used Perdew and Zunger's[24] parametrization of the density functional based on the results of Ceperley and Alder.[25] The generalized gradient corrections of Becke[26] and Perdew[27] were applied. For solving the electronic structure problem, a plane wave cutoff of 30 Ry was used for the wave functions, while the electron density was represented with a cutoff of 60 Ry. Projector functions of the s type for hydrogen atoms and s, p, and d projectors for all other atoms were included in the calculations. For the sake of comparison with other more common quantum chemical methods, selected bond lengths and angles calculated at different levels of theory[28] are summarized in Table 1, along with the corresponding data determined by microwave spectroscopy. Table 1 also includes experimental[4] and calculated ν(OH) frequencies and the energy differences ΔE between the C_s equilibrium ground states and the symmetrical C_{2v} states, which give an estimate of the height of the proton-transfer barrier. The gradient corrections according to Becke and Perdew slightly overestimate the strength of a hydrogen-bonding interaction with respect to the associated covalent bond, and our proton-transfer barrier height may be somewhat too low by a factor of about two or three. Since we are mainly interested in qualitative features and in a qualitative picture of the proton-transfer processes, this accuracy should be adequate. Moreover, an excellent agreement between the experimental ν(OH) frequency and that calculated by PAW (Table 1) is found, and a similarly good agreement is also observed for the ν(CH) frequencies. This indicates that our force field is realistic and that the calculations are an appropriate tool for obtaining a qualitative picture of the proton-transfer process at finite temperatures. To evaluate the most important molecular parameters that govern the proton-transfer process, that is, those that can distinguish between transition and nontransition periods, a sample data set of 1380 points from our trajectories was analyzed by standard statistical methods (discriminant analysis) and with the aid of a neural network. Both the discriminant analysis and the neural network classify sets of parameters or objects into certain categories (here: transitions or nontransitions). The discriminant analysis determines a linear combination of relevant parameters, which can predict to which category new cases belong. To prevent the discriminant analysis from simply fitting the function to reproduce the given data, the data was split into the learn and test subsets. The former was used to build up the discriminating function, whereas the latter had the task of proving whether the function correctly classifies independent data. In the case of the neural network, the discriminating function was not just a linear combination of the relevant parameters, but was built up by sigmoid functions, which can determine any nonlinear relationship. The neural network was a three-layer feedforward network trained by backpropagation.[29] Part of the data (44 %) was used for training, a smaller independent data set (12 %) was used to decide when to stop the training process, and the remaining data formed the independent test set, which shows how well the neural network deals with new cases.

Table 1. Selected bond lengths [Å] and angles [°], proton transfer barriers [kJ mol^{-1}], and ν(OH) frequencies [cm^{-1}] of malonaldehyde, as obtained from experimental and theoretical data.

	Exp.[a]	HF[b]	MP2[b]	B3LYP[b]	BLYP[b]	B3P86[b]	PAW
O – H	(0.969)	0.956	0.994	1.007	1.035	1.020	1.058
O ··· H	(1.680)	1.881	1.695	1.641	1.588	1.556	1.525
O ··· O	2.553	2.682	2.591	2.554	2.544	2.497	2.511
C – O	1.320	1.312	1.329	1.319	1.330	1.309	1.322
C=C	1.348	1.342	1.363	1.369	1.384	1.370	1.377
C – C	1.454	1.453	1.440	1.437	1.440	1.428	1.423
C=O	1.234	1.207	1.250	1.246	1.265	1.246	1.266
O – H ··· O	147.6	139.6	147.5	148.5	150.9	150.9	152.5
C-O-H	106.3	109.4	105.3	105.4	104.2	104.6	103.3
C=O ··· H		99.7	99.4	99.9	99.6	100.1	99.7
O-C=C	124.5	126.2	124.5	123.9	123.4	123.3	122.9
C-C=O	123.0	124.2	123.5	123.5	123.3	123.2	122.9
C-C=C	119.4	120.9	119.5	118.8	118.6	118.0	118.7
ΔE[c]	(6.6)	43.0	15.2	9.7	5.6	6.1	4.9
ν(OH)	2860[d]	3941[e]	3318[e]	3035[e]	2660[e]	2819[e]	2850[f]

[a] From microwave data[3] (except for ν(OH)). [b] 6-31G(d,p) basis set. [c] Energy difference between C_{2v} transition state and C_s equilibrium structure (kJ mol^{-1}). [d] IR frequency from CCl_4 solution. [e] Harmonic frequency. [f] From the R(OH) autocorrelation function.

Results and Discussion

PAW trajectories: Figure 2 shows 2.4 ps time evolutions of the O_A – H, O_B – H, and O – O distances at various temperatures between 325 and 600 K. The proton-transfer processes are clearly apparent from the crossover points of the two R(OH) time evolutions. As expected, with increasing temperature, the transfer rates significantly increase to about 10 ps^{-1} at 500 K and to about 25 ps^{-1} at 600 K (no transitions were observed below 325 K), which compares with the experimentally determined tunneling rate of only about 1 ps^{-1}.[3] This indicates that proton tunneling, which is not taken into account by our calculations, adds at most only quantitative corrections to the dynamics. In principle, the temperature dependence of the transfer rates could be used to evaluate a transition-state energy, but owing to the limited time periods of our trajectories, the statistical significance of the simulations is insufficient for obtaining a statistically reliable value. Moreover, since proton transfer is clearly not a simple statistical process (see below), the

0947-6539/98/0408-1420 $ 17.50+.50/0 *Chem. Eur. J.* **1998**, *4*, No. 8

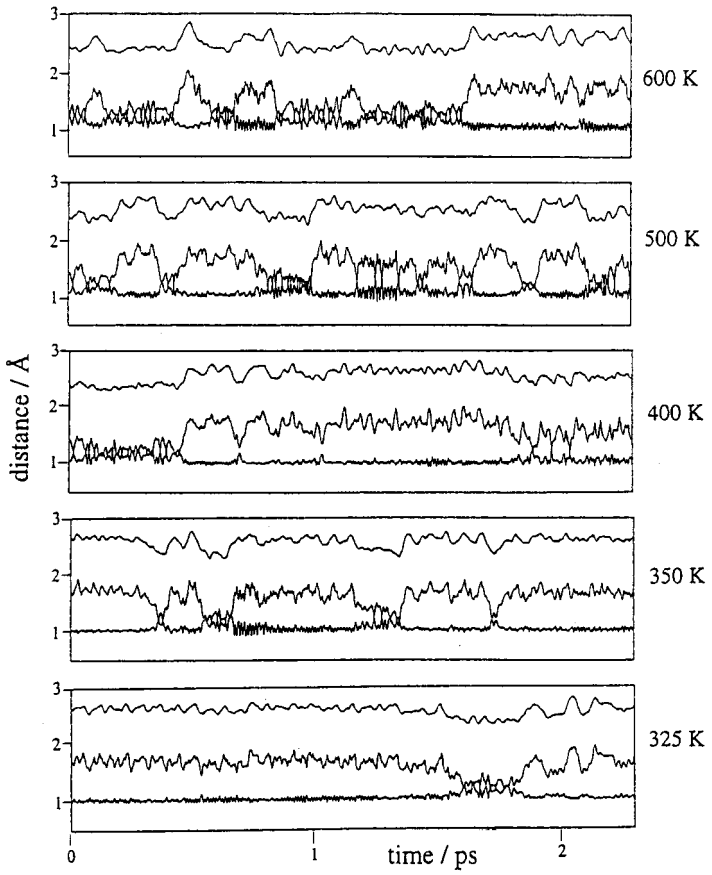

Figure 2. O_A-H and O_B-H distances (lower traces) and O–O distance (upper trace) versus time at different temperatures.

physical meaning of a transition-state energy derived from an Arrhenius-like plot is not entirely evident.

Figure 3 depicts the changes of the molecular geometry over a 20 fs time period for a single proton-transfer transition

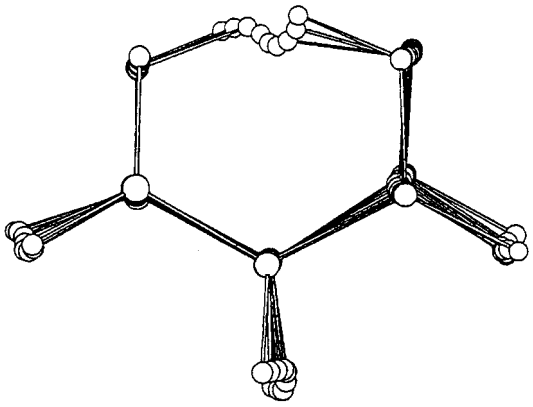

Figure 3. Snapshots of the geometry of malonaldehyde during a proton transfer transition (time intervals: 2.4 fs).

and gives an impression of the full dynamic behavior of the molecule. Even within this rather short time, not only the hydrogen atoms, but also the heavy atoms, exhibit appreciable motion, and a proper description of proton transfer requires many, if not all, of the 21 internal degrees of freedom of the molecule. This is partially taken into account in Figure 4, which displays a blow up of 0.48 ps of the 500 K time evolutions shown in Figure 2 and the time evolutions of some

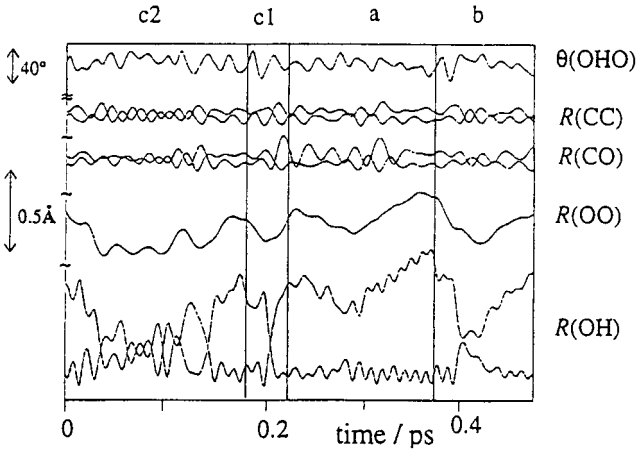

Figure 4. Time evolutions of several molecular parameters at 500 K showing: a normal period (a), a near-transition (b), an isolated transition (c1), and consecutive shuttling transitions (c2).

additional geometric parameters. From Figure 4, one can (somewhat arbitrarily) distinguish four different situations with respect to the proton motion: a) normal periods, in which the proton remains firmly trapped at one oxygen atom, b) near-transitions, in which the two O–H distances become very similar, but no proton transfer takes place, c1) isolated transitions that correspond to a single proton transfer, and c2) proton shuttling periods with multiple, consecutive transitions. The distinction between isolated and shuttling transitions is similar to Hutchinson's distinction between single-crossing events and quasi-periodic oscillations.[17]

Analysis of geometric data: For a more detailed analysis, a sample data set consisting of three classes, each of which contained the molecular parameters of 460 single time steps of the 500 K PAW trajectory, was constructed: all of the 92 isolated and the shuttling proton transfer transitions that occurred during the simulation, each characterized by the crossover point and four preceding time steps (class c); the 92 most significant near-transitions, characterized by the turning points[30] of the R(OH) time evolutions and by their preceding four time steps (class b); and 92 points that were arbitrarily chosen from the normal periods along with their preceding four time steps (class a). Table 2 summarizes the average values and ranges of selected bond lengths and angles for the three classes. Within the normal periods (class a) the average geometry is similar to the equilibrium geometry at $T=0$ K with a strongly asymmetric hydrogen bond and distinctly different C–O distances and C–C distances. In contrast, the average geometry of the crossover points of the transitions (class c) is close to the C_{2v}-symmetric transition state that emerges from zero-point calculations, with a rather short O–O distance and almost equal C–O distances and C–C distances. However, from the ranges given in Table 2, it is evident that the geometries of the individual crossover points can significantly deviate from this average geometry. Hence, the finite-

Table 2. Mean values and ranges (in parentheses) of selected bond lengths [Å] and angles [°] of the points included in the sample set used for data analysis (see text): a) points of normal periods, b) turning-points of near-transitions, and c) crossover-points of proton transfer transitions.

	a	b	c
O···O	2.64 (2.49–2.80)	2.53 (2.36–2.70)	2.38 (2.25–2.59)
C–O	1.34 (1.31–1.44)	1.33 (1.28–1.40)	1.30 (1.25–1.37)
C=C	1.38 (1.30–1.50)	1.38 (1.29–1.50)	1.41 (1.32–1.50)
C–C	1.44 (1.34–1.56)	1.44 (1.35–1.53)	1.41 (1.33–1.50)
C=O	1.26 (1.19–1.33)	1.27 (1.22–1.31)	1.30 (1.23–1.36)
O–H···O	145 (129–165)	151 (139–169)	155 (146–169)
C-O-H	105 (95–116)	102 (92–111)	102 (91–111)
C=O···H	98 (88–106)	100 (90–110)	102 (92–111)
O–C=C	123 (115–131)	123 (114–132)	121 (113–128)
C–C=O	123 (116–133)	123 (114–131)	121 (113–128)
C–C=C	121 (113–128)	118 (111–125)	116 (109–125)

temperature PAW simulations do not yield a well-defined transition state corresponding to a preferred bottleneck-like reaction path for the proton-transfer processes; instead, they indicate a more complicated situation. This is not unexpected, because at the temperatures considered the total kinetic energy of the molecule is about 40 kJ mol^{-1} and the dynamics is expected to be rather complex. Consequently, the question arises whether there are systematic relationships between combinations of molecular parameters and the occurrence of proton-transfer processes, or at least, whether those parameters can be determined which most prominently govern the probability of proton transfer.

Among the geometric parameters that govern the proton-transfer process, the O–O distance is the most important. A plot of R(OO) versus R(OH) of the points in the sample set shows that most proton-transfer transitions are associated with small O–O distances (Figure 5). Up to about

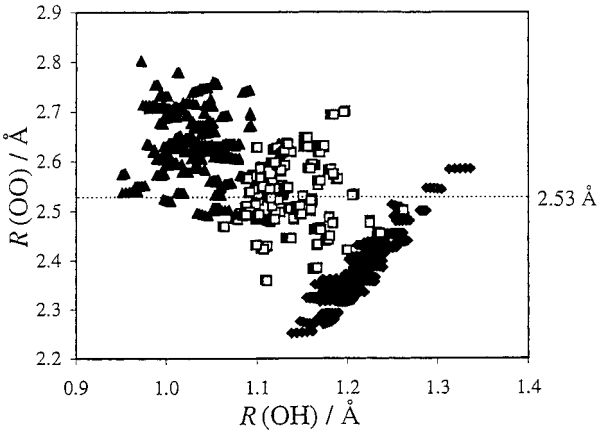

Figure 5. R(OO) versus R(OH) for the points used for data analysis (see text): ▲ normal periods, □ near-transitions, ◆ proton-transfer transitions.

98.5% of the points belonging to classes a (normal regions) and c (transitions) are distinguished correctly by a limiting distance of 2.53 Å (dotted horizontal line in Figure 5), and 91.5% of the points are still correctly classified if a distinction is made between classes a+b (nontransitions = normal regions+near-transitions) and class c (transitions). The underlying reason for the crucial role of the O–O distance was demonstrated in a recent ab initio study at the MP2/6-31G** level of theory,[10] in which potential energies were calculated as a function of increasing O–H distance (i.e., for hypothetical proton transfer transitions) at fixed O–O distances, but with otherwise full geometry optimization. For the equilibrium O–O distance, the well-known double-minimum potential was obtained, and the two minima were separated by an energy barrier of about 40 kJ mol^{-1}. For shorter O–O distances the barrier decreased, and it vanished below 2.3 Å to give a symmetric single-minimum potential. We have performed similar point-to-point potential energy calculations for such hypothetical proton-transfer transitions at fixed O–O distances with the PAW program; in our case the proton-transfer reaction coordinate was defined by $\rho = [R(O_AH) - \cos\theta(O_BO_AH)]/R(OO)$.[31] In Figure 6 the results are displayed for three representative O–O distances. At 2.80 Å, which is close to the upper limit of the O–O distances in our simulations, the two minima are separated by a potential energy barrier of 66 kJ mol^{-1}, which exceeds the total kinetic

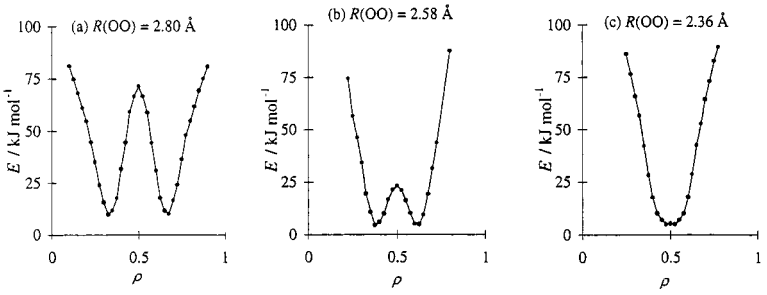

Figure 6. Potential energy as a function of the proton reaction coordinate ρ[31] with fixed O–O distances but otherwise full geometry optimization.

energy of the molecule at 500 K (50 kJ mol^{-1}). At 2.58 Å, which is the upper limit observed for crossover points of isolated transitions, the barrier decreases to 19 kJ mol^{-1}, while at 2.36 Å, which is the mean value of shuttling transitions, an almost perfect single-minimum potential is obtained. Note that these model calculations can not represent real proton-transfer transitions because of the assumption of fixed O–O distance. However, they clearly indicate that, depending on the O–O distance, the energetic preconditions for proton-transfer processes and therefore the probability of proton transfer can differ widely. At large O–O distances (Figure 6a) proton transfer should be almost impossible, at medium distances (Figure 6b) it should be a rare event, and at short distances (Figure 6c) proton transfer should degenerate to a large-amplitude ν(OH) vibration of a (nearly) symmetric O···H···O hydrogen bond.

Although the O–O distance is an important factor governing the proton motion, a short O–O distance is neither a necessary nor a sufficient criterion for proton transfer: distances of up to 2.586 Å are found for the crossover points, but as short as 2.490 Å in the normal regions, and even as short as 2.358 Å for the turning points of the near-transitions. Therefore, we performed a multidimensional analysis of our

0947-6539/98/0408-1422 $ 17.50+.50/0 Chem. Eur. J. 1998, 4, No. 8

sample data set by discriminant analysis and with a neural network. The aim was to identify the parameters which in combination with the O–O distance would provide the most reliable distinction between classes a, b, and c. Besides purely geometric parameters, the analysis also included dynamic parameters that were defined by the changes of geometric parameters with respect to the preceding time steps. Without going into details, some basic results are shown in Figure 7.

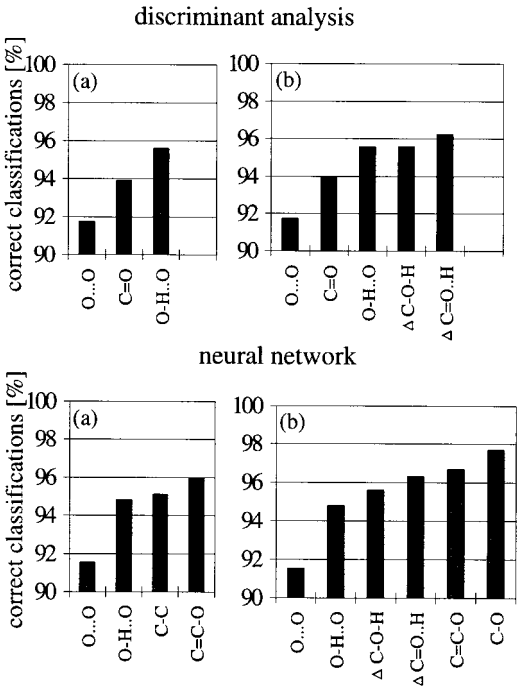

Figure 7. Percentage of correct classifications of nontransitions and transitions obtained by discriminant analysis and with the neural network by successive inclusion of parameters: geometric parameters (a), and geometric plus dynamic parameters (b).

Here we restrict ourselves to the discrimination between the combined classes a+b (nontransitions) and class c (transitions). In an initial approach (Figure 7a), only geometric parameters were considered: five distances (O···O, C–O, C–C, C=C, C=O), six angles (C=C–O, C–C=O, C–C=C, O–H···O, C–O–H, C=O···H), and four torsion angles (C–C=C–O, C=C–C=O, C=C–O–H, C–C=O···H). Both the discriminant and network analyses yielded about 95% correct classifications, which is moderately better than the 91.5% correct classifications based on the O–O distance alone. For both methods, only two or three parameters besides R(OO) are relevant. In a second approach (Figure 7b), the changes Δ of the above 15 parameters relative to the preceding time step were also included, and the correct classifications increased by about 1% for both analyses. The parameters regarded as relevant by the two methods differ in part and are therefore not fully independent. Hence, they can be partly replaced by one other. As expected, these parameters are distances and angles within the hydrogen-bonded chelate ring and changes therein. With both methods, the changes in the two C–O–H angles enter the discrimination functions as relevant dynamic parameters, but it is not clear whether the changes in these angles directly influence the proton-transfer process, or whether they are purely a consequence of the process.

Finally, the discriminating functions that emerged from the analysis were used to classify all time steps of the trajectories as transitions or nontransitions. An example is given in Figure 8, which shows a 2.42 ps window of the 500 K time evolutions of the two O–H distances with the classifications of the time steps. This analysis showed that not only the

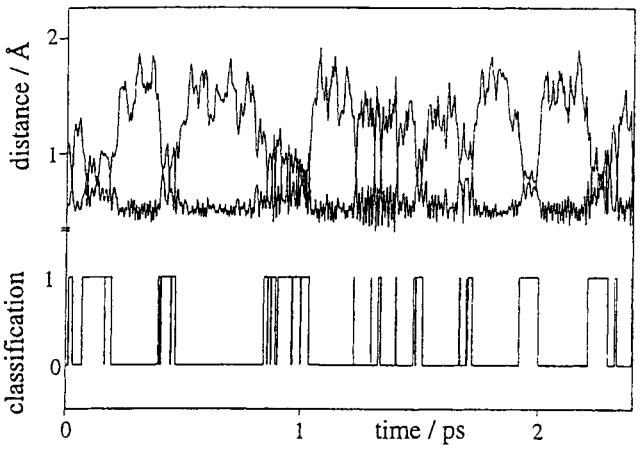

Figure 8. O–H distances versus time at 500 K and classification of the points as transitions (1) or nontransitions (0).

crossover points and the four preceding time steps that were included in the sample set, but that all points within a longer time period (about 100 fs or more) are also classified as transitions. Therefore, within the accuracy limits of the analysis function, we can define a proton-transition period during which the molecule has a geometry that is favorable for proton transfer.

In summary, although both methods are capable of identifying parameters that determine the proton-transfer process, they fail to predict definite requirements for the transfer to occur. Possible reasons are that the situations are too complex and variable for an exact analysis or that the analysis did not consider all relevant factors (see below).

Energetic considerations: Since the analysis of geometric data did not provide fully satisfactory results regarding the requirements for proton-transfer processes, we tried another approach to obtain a better understanding of the driving forces that govern the proton motion. Model calculations were performed in the following way: 1) a molecular geometry was taken from a single time step of a PAW trajectory; 2) except for the proton under consideration, all atoms were fixed (this is the main difference to the calculations of Figure 6); 3) the proton under consideration was moved step by step along the proton-transfer reaction coordinate ρ;[31] 4) under these constraints (i.e., a given ρ value and an otherwise fixed geometry), the proton position was optimized for each step of ρ, and the potential energy was calculated. The resulting potential $E(\rho)_t$ represents the energetic preconditions for a hypothetical motion of the proton between the two oxygen atoms within a heavy–light–heavy atom approximation[32] (i.e., under the assumption that

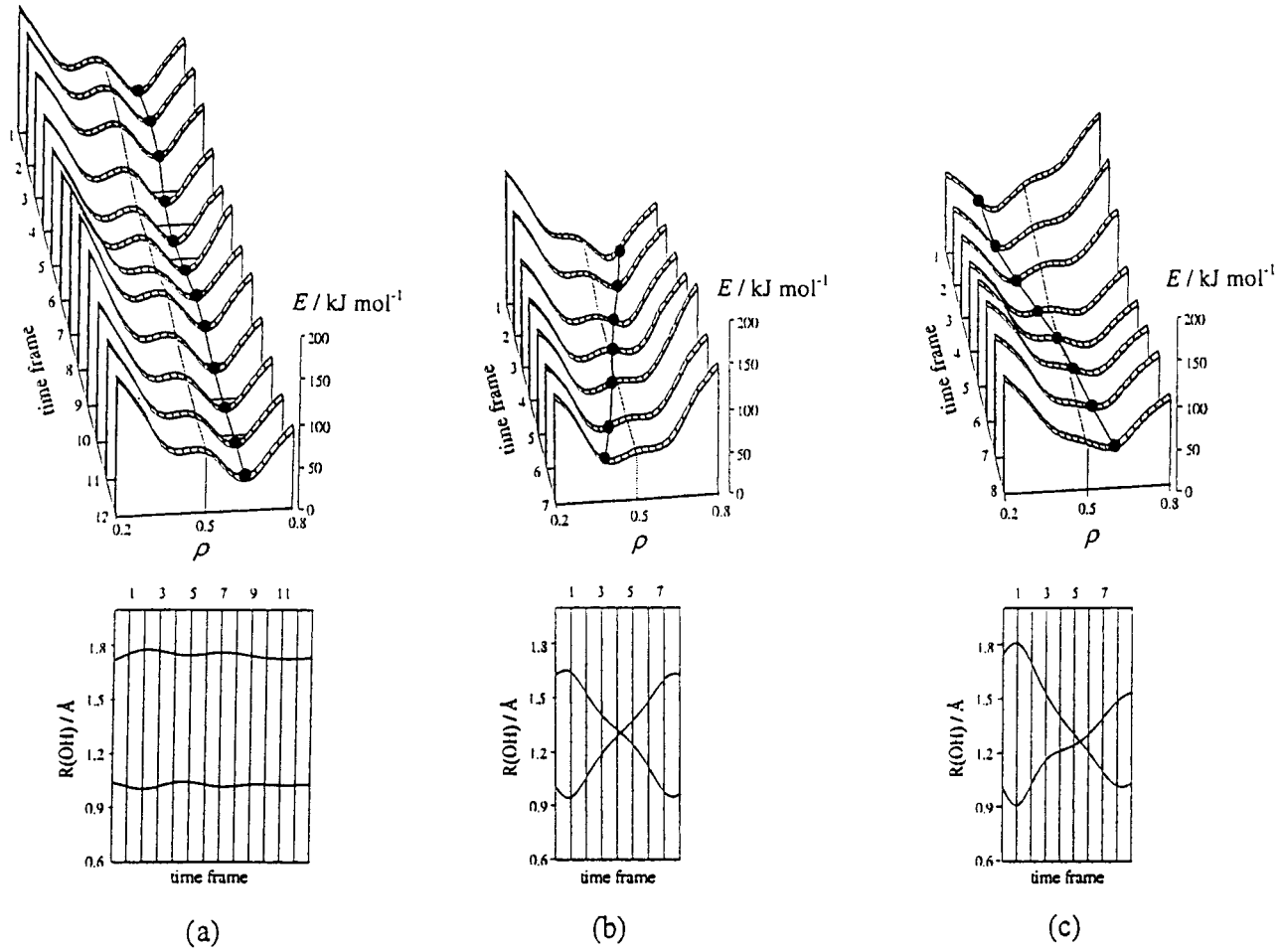

Figure 9. Potential energy as a function of the proton reaction coordinate ρ[31] with otherwise fixed geometry for consecutive time frames at intervals of 2.42 fs and the corresponding R(OH) time evolutions of a normal period (a), two isolated transitions (b,c), two shuttling region regions (d,e), and a near transition (f).

the motion of the proton is much faster than that of all other atoms). As such a Born–Oppenheimer-like approximation is rather poor in our case (the heavy atom to light atom mass ratio is only around ten), the potential $E(\rho)_t$ could more realistically be interpreted in terms of the potential experienced by the proton at the time step just considered. This potential should govern the next step(s) of its motion between the two oxygen atoms; if we neglect the kinetic energy of the proton, then to a first approximation, the proton should follow the $E(\rho)_t$ gradient.

We calculated such $E(\rho)_t$ potentials for several consecutive time frames from selected regions of the PAW trajectories and thus obtained the time evolutions of the potential energy that governs the proton motion along the proton-transfer reaction coordinate ρ for the selected time periods. In Figure 9 such $E(\rho)_t$ time evolutions are shown by staggered plots of single time frames with 2.4 fs time intervals for six instances taken from the 500 K trajectory. These correspond to the four typical situations shown in Figure 4. The actual proton positions for each time frame, as they emerged from the trajectory, are indicated by filled circles and depict the proton motion within the considered time period. Additionally, the time evolutions of the two O–H distances are shown; the vertical lines indicate the time frames of the staggered plots.

Figure 9a shows 12 snapshots of a normal region. Within the entire time period (26.6 fs) we obtain the asymmetric double-minimum potentials that are characteristic of moderately strong hydrogen bonds. The potential $E(\rho)_t$ is approximately constant, the proton remains firmly attached at one oxygen atom, and its motion corresponds to a stationary, high-frequency, low-amplitude ν(OH) vibration. As already noted above, the PAW-calculated frequency of this motion is 85.5 THz (2850 cm^{-1}), which almost exactly matches the experimental ν(OH) frequency of 2860 cm^{-1}. Such a frequency is characteristic for moderately strong, but clearly asymmetric intramolecular O–H···O hydrogen bonds with an equilibrium O–O distance of about 2.55 Å.

Figures 9b and 9c display seven and eight snapshots of two isolated transitions with total time periods of 14.5 and 16.9 fs, respectively. The potential-energy evolutions start with a strongly asymmetric potential whose minimum is located at one oxygen atom. This is the usual situation in the normal regions, where the proton is trapped in one tautomeric form. In the following steps, the potential rapidly changes to a shallow double-minimum potential and then again becomes

0947-6539/98/0408-1424 $ 17.50+.50/0 *Chem. Eur. J.* **1998**, *4*, No. 8

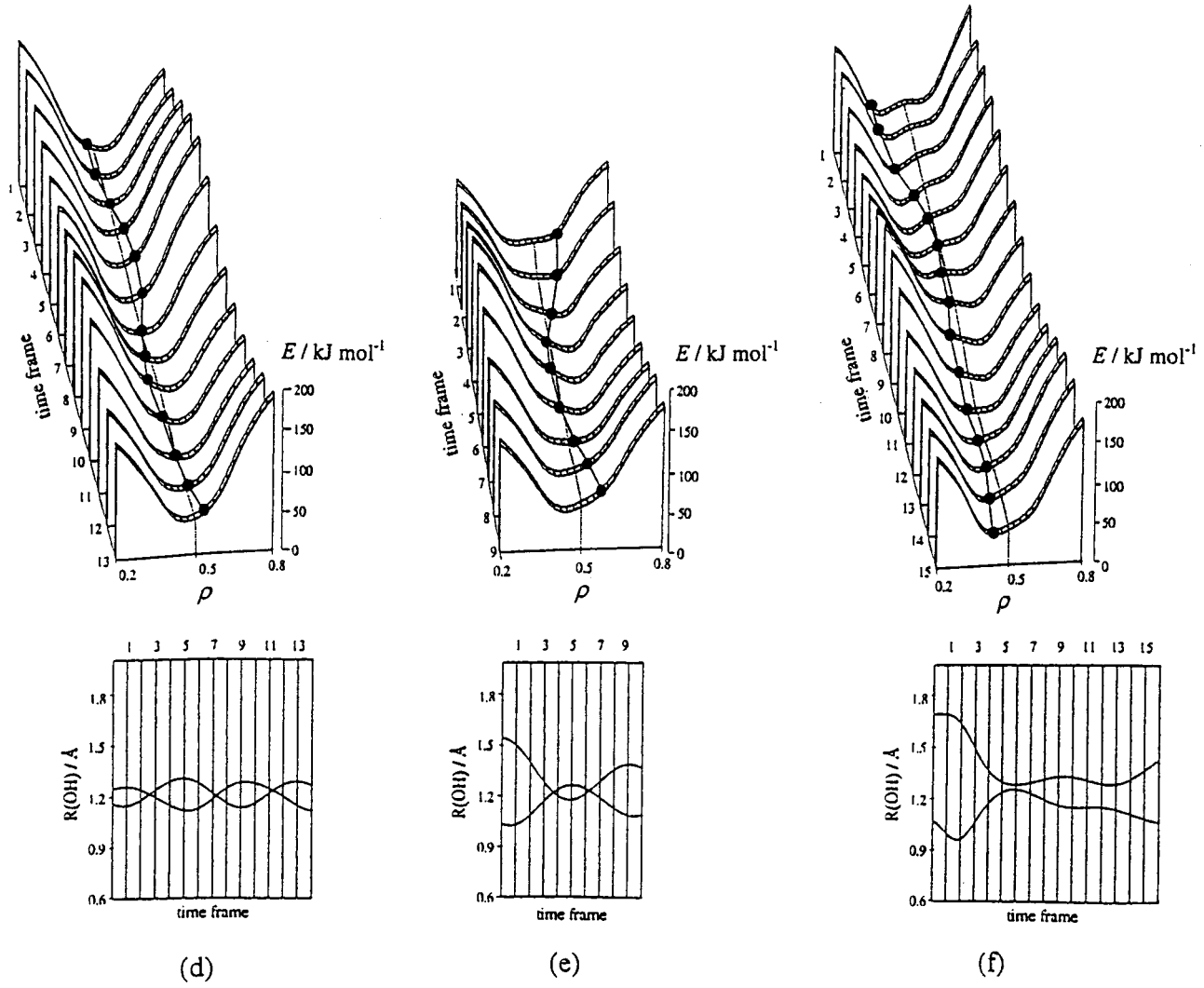

strongly asymmetric, but with the minimum located at the other oxygen atom. While the proton moves uphill (frames 3, 4 and 4, 5), the barrier decreases and the potential changes in such a way that the proton falls into the new minimum at the other oxygen atom (frames 5–7 and 6-8). The changes in the shape of the potential $E(\rho)_t$ that drive the proton-transfer process occur within a time period not longer than that of a single ν(OH) vibration.

Figures 9d and 9e display 13 and 9 potential energy snapshots (time periods: 29 and 19.4 fs) taken from two shuttling periods. These situations differ significantly from those of Figures 9b and 9c in having more or less symmetric single-minimum potentials that undergo only minor changes during the entire time periods considered. In these cases the proton motion is not a true proton transfer, but rather a (quasi)stationary, low-frequency, large-amplitude vibration, which takes place as long as the single minimum potential persists (i.e., as long as the geometry remains favorable). The average frequency of the periodic proton motion within the shuttling regions of 61.5 THz corresponds to a ν(OH) frequency of about 2050 cm^{-1}.

Figure 9f shows 15 snapshots from a region that covers a near-transition. The potential-energy evolution starts with an asymmetric double-minimum potential with the minimum at the left oxygen atom O_A, displays a series of symmetric double-minimum potentials and single-minimum potentials, and ends with a strongly asymmetric single-minimum potential whose minimum is again located at O_A. The actual proton motion makes this picture particularly interesting. At frame 6 the proton comes close to the crossover point ($\rho = 0.5$), but it follows the potential energy gradient and turns back just before the potential becomes favorable for proton transfer (frames 8–11). At frames 12 and 13, where the proton again comes close to $\rho = 0.5$, the potential has already changed such that the proton remains trapped at O_A. Figure 9f clearly shows that a proton-transfer transition is not only governed by certain potential energy situations that are directly related to the geometry of the rest of the molecule, but also depends on the current position of the proton and, in particular, on the current direction of its momentum. The latter finding is not surprising and is probably one reason why the statistical analysis in which proton position and momentum were not explicitly considered did not give better results.

Let us finally consider the difference between isolated proton-transfer transitions and proton-shuttling periods, which in Figure 4 were distinguished from a purely visual

view point. From Figure 9 it is evident that this discrimination seems to be physically meaningful. Isolated transitions and proton-shuttling transitions represent two extreme cases, while the actually observed proton transfers range from purely isolated transitions, through borderline cases, to clear shuttling processes. Within the framework of our model, both isolated and shuttling transitions are associated with a change of the normally strongly asymmetric potential $E(\rho)_t$ to a nearly symmetric double- or single-minimum potential. In the first case the usual asymmetric potential is rapidly reestablished (within a time shorter than a ν(OH) vibrational cycle), whereas in the latter case it takes a distinctly longer time (more than two ν(OH) vibrational cycles). What is more, isolated transitions and shuttling periods also represent two borderline cases with respect to geometric parameters, especially the O – O distance. Table 3 lists the mean values and standard deviations of selected bond lengths and angles for the eight most representative crossover points of isolated and shuttling transitions. On average, R(OO) is larger by about 0.13 Å for isolated than for shuttling transitions.

Table 3. Mean values and standard deviations (in parentheses) of selected bond lengths [Å] and angles [°] for clearly isolated and shuttling transitions (see text).

	Isolated	Shuttling
O ··· O	2.49(6)	2.36(2)
C – O	1.30(2)	1.30(2)
C=C	1.40(4)	1.42(3)
C – C	1.40(4)	1.42(5)
C=O	1.30(3)	1.31(2)
O – H ··· O	156(5)	158(4)
C-O-H	101(3)	101(3)
C=O ··· H	97(4)	102(3)
O – C=C	119(2)	120(3)
C – C=O	123(2)	119(2)
C – C=C	120(2)	117(3)

Summary and Conclusions

We have performed ab initio PAW molecular dynamics calculations on malonaldehyde at temperatures between 1 and 600 K that shed some new light on proton motion and proton transfer. Our conclusions are as follows:

Within the framework of the PAW approach, which neglects quantum effects, proton transfer is described as a dynamic process that results from the full dynamics of the molecule. At elevated temperatures, proton transfer is not associated with a well-defined transition state and a corresponding preferred reaction path, but takes place in various, widely differing geometrical situations. Due to the molecular dynamics, the molecular geometry permanently changes, and sometimes situations occur that are favorable for proton transfer.

Although it was not possible to clearly specify the requirements and preconditions for proton transfer for each event by using appropriate analysis methods (discriminant analysis, neural network) we found the most relevant molecular parameters for distinguishing periods of transitions and periods of nontransitions with an accuracy greater than 95 %. As expected, a short O – O distance proved to be the most important parameter, but a limiting O – O distance is neither a necessary nor a sufficient condition.

Two extreme situations of proton transfer can be discriminated: statistical isolated transitions and nonstatistical shuttling transitions, which represent the limits of long and short O – O distances, respectively. In the first case, proton transfer remains a single event in which the proton is trapped at one oxygen atom at the beginning and at the other oxygen atom at the end. The second case is characterized by multiple consecutive proton-transfer transitions that correspond to a (quasi)stationary, large-amplitude, low-frequency motion.

The actual proton motion that emerges from the PAW calculations can be reasonably well understood in terms of the time evolution of the potential energy along an appropriately chosen proton-transfer reaction coordinate. At any time, this potential is determined by the current molecular geometry, which permanently changes due to the dynamics of the molecule. Isolated transitions start with an asymmetric potential (i.e., the proton is firmly located at one oxygen), pass through a series of nearly symmetric, broad potentials, and end with another asymmetric potential whose minimum is now located at the other oxygen atom. Proton shuttling processes are associated with a more or less symmetric single-minimum potential that persists for a longer time period without significant changes, and the proton undergoes a (quasi)stationary motion within this potential.

In addition to the necessary potential energy conditions, for proton transfer to occur, favorable position and momentum of the proton are also required.

Acknowledgments: The authors are grateful to Dr. P. Blöchl, IBM research division, Zürich, for valuable help and discussion. The work was supported by the Jubiläumsfonds der Österreichischen Nationalbank, Projekt Nr. 5701, by the Fonds zur Förderung der Wissenschaftlichen Forschung in Österreich, Projekt Nr. 10842, and by the IBM Joint Research Project 83470512. Supply of computer facilities by the computer center of the University of Vienna is kindly acknowledged.

Received: January 5, 1998 [F952]

[1] K. Wolf, W. Mikenda, *J. Mol. Struct. (Special edition: Proceedings of the XIIth Conference-Workshop Horizons in Hydrogen Bond Research, Niederöblarn, Austria, 1997)*, in press.

[2] a) S. H. Bertz, G. Dabbagh, *J. Org. Chem.* **1990**, *55*, 5161; b) J. S. Craw, M. A. C. Nascimento, *Chem. Phys. Lett.* **1990**, *168*, 423; c) N. N. Shapet'ko, S. S. Brestova, G. M. Lukovkin, Y. S. Bogachev, *Org. Mag. Res.* **1975**, *7*, 237; d) R. S. Brown, A. Tse, T. Nakashima, R. C. Haddon, *J. Am. Chem. Soc.* **1979**, *101*, 3157. e) R. S. Brown, *J. Am. Chem. Soc.* **1977**, *99*, 5497; f) C. J. Seliskar, R. E. Hoffman, *Chem. Phys. Lett.* **1976**, *43*, 481; g) W. O. George, V. G. Mansell, *J. Chem. Soc. B* **1968**, 132.

[3] a) P. Turner, S. L. Baughcum, S. L. Coy, Z. Smith, *J. Am. Chem. Soc.* **1984**, *106*, 2265; b) S. L. Baughcum, Z. Smith, E. B. Wilson, R. W. Duerst, *J. Am. Chem. Soc.* **1984**, *106*, 2260; c) S. L. Baughcum, R. W. Duerst, W. F. Rowe, Z. Smith, E. B. Wilson, *J. Am. Chem. Soc.* **1981**, *103*, 6296; d) W. F. Rowe, Jr., R. W. Duerst, E. B. Wilson, *J. Am. Chem. Soc.* **1976**, *98*, 4021.

[4] a) S. H. Bauer, C. F. Wilcox, *Chem. Phys. Lett.* **1997**, *279*, 122; b) D. W. Schiering, J. E. Katon, *Appl. Spectr.* **1986**, *40*, 1049; c) Z. Smith, E. B. Wilson, R. W. Duerst, *Spectrochim. Acta* **1983**, *39A*, 1117; d) C. J. Seliskar, R. E. Hoffmann, *J. Mol. Spectr.* **1982**, *96*, 146.

[5] a) T. Chiavassa, P. Verlaque, L. Pizzala, A. Allouche, P. Roubin, *J. Phys. Chem.* **1993**, *97*, 5917; b) T. Chiavassa, P. Roubin, L. Pizzala, P. Verlaque, A. Allouche, F. Marinelli, *J. Phys. Chem.* **1992**, *96*, 10659; c) P. Roubin, T. Chiavassa, P. Verlaque, L. Pizzala, H. Bodot, *Chem.*

  0947-6539/98/0408-1426 $ 17.50+.50/0

Phys. Lett. **1990**, *175*, 655; d) D. W. Firth, P. F. Barbara, H. P. Trommsdorff, *Chem. Phys.* **1989**, *136*, 349.
[6] D. W. Firth, K. Beyer, M. A. Dvorak, S. W. Reeve, A. Grushow, K. R. Leopold, *J. Chem. Phys.* **1991**, *94*, 1812.
[7] a) K. B. Wiberg, J. Ochterski, A. Streitwieser, *J. Am. Chem. Soc.* **1996**, *118*, 8291; b) K. Luth, S. Scheiner, *J. Phys. Chem.* **1994**, *98*, 3582; c) K. Luth, S. Scheiner, *Int. J. Quant. Chem: Quant. Chem. Symp.* **1993**, *27*, 419; d) K. B. Wiberg, C. M. Hadad, T. J. LePage, C. M. Breneman, M. J. Frisch, *J. Phys. Chem.* **1992**, *96*, 671; e) M. A. Rios, J. Rodriguez, *J. Mol. Struc. (Theochem)* **1991**, *228*, 149; f) G. Buemi, *J. Mol. Struc. (Theochem)* **1990**, *208*, 253; g) G. Buemi, C. Gandolfo, *J. Chem. Soc. Faraday Trans. 2* **1989**, *85*, 215; h) M. J. Frisch, A. C. Scheiner, H. F. Schaefer III, *J. Chem. Phys.* **1985**, *82*, 4194; i) S. Millefiori, A. Millefiori, G. Granozzi, *J. Mol. Struc. (Theochem)* **1983**, *105*, 135; j) P. George, C. W. Bock, M. Trachtman, *J. Comput. Chem.* **1980**, *1*, 373; k) F. Sim, A. St-Amant, I. Papai, D. R. Salahub, *J. Am. Chem. Soc.* **1992**, *114*, 4391; l) J. S. Binkley, M. J. Frisch, H. F. Schaefer III, *Chem. Phys. Lett.* **1986**, *126*, 1.
[8] V. Barone, C. Adamo, *J. Chem. Phys.* **1996**, *105*, 11007.
[9] J. Bicerano, H. F. Schaefer III, W. H. Miller, *J. Am. Chem. Soc.* **1983**, *105*, 2550.
[10] G. Buemi, F. Zuccarello, *J. Chem. Soc. Faraday Trans.* **1996**, *92*, 347.
[11] a) Z. Latajka, S. Scheiner, *J. Phys. Chem.* **1992**, *96*, 9764; b) N. Shida, J.Almöf, P. F. Barbara, *J. Phys. Chem.* **1991**, *95*, 10457.
[12] a) V. A. Benderskii, D. E. Makarov, *Chem. Phys.* **1993**, *170*, 275; b) E. Bosch, M. Moreno, J. M. Lluch, *J. Am. Chem. Soc.* **1992**, *114*, 2072; c) Y. Chang, W. H. Miller, *J. Phys. Chem.* **1990**, *94*, 5884; d) E. Bosch, M. Moreno, J. M. Lluch, J. Bertran, *J. Chem. Phys.* **1990**, *93*, 5685; e) T. Carrington, Jr., W. H. Miller, *J. Chem. Phys.* **1986**, *84*, 4364.
[13] a) V. A. Benderskii, E. V. Vetoshkin, S. Y. Grebenshchikov, L. von Laue, H. P. Trommsdorff, *Chem. Phys.* **1997**, *219*, 199; b) Z. Smedarchina, W. Siebrand, M. Z. Zgierski, *J. Chem. Phys.* **1995**, *103*, 5326; c) V. K. Babamov, *Chem. Phys. Lett.* **1994**, *217*, 254; d) S. Takada, H. Nakamura, *J. Chem. Phys.* **1994**, *100*, 98; e) P. Bala, B. Lesyng, J. A. McCammon, *Chem. Phys.* **1994**, *180*, 271; f) Y. Guo, T. D. Sewell, D. L. Thompson, *Chem. Phys. Lett.* **1994**, *224*, 470; g) N. Shida, P. F. Barbara, J. E. Almöf, *J. Chem. Phys.* **1989**, *91*, 4061.
[14] N. Makri, W. H. Miller, *J. Chem. Phys.* **1989**, *91*, 4026.
[15] T. D. Sewell, Y. Guo, D. L. Thompson, *J. Chem. Phys.* **1995**, *103*, 8557.
[16] a) T. Komatsuzaki, M. Nagaoka, *Chem. Phys. Lett.* **1997**, *265*, 91; b) T. Komatsuzaki, M. Nagaoka, *J. Chem. Phys.* **1996**, *105*, 10838.
[17] J. S. Hutchinson, *J. Phys. Chem.* **1987,** *91*, 4495.
[18] a) H. Lampert, W. Mikenda, A. Karpfen, *J. Phys. Chem.* **1997**, *101*, 2254; b) H. Lampert, W. Mikenda, A. Karpfen, *J. Phys. Chem.* **1996**, *100*, 7418.
[19] P. E. Blöchl, *Phys. Rev. B* **1994**, *50*, 17953.
[20] R. Car, M. Parrinello, *Phys. Rev. Lett.* **1985,** *55*, 2471.
[21] a) K. Schwarz, E. Nusterer, P. Margl, P. E. Blöchl, *Int. J. Quant. Chem.* **1997,** *61*, 369; b) E. Nusterer, K. Schwarz, P. E. Blöchl, *Angew. Chem.* **1996,** *108*, 187; *Angew. Chem. Int. Ed. Engl* **1996,** *35*, 175.
[22] a) J. C. Caulfield, A. J. Fisher, *J. Phys. Condens. Matter* **1997**, *9*, 3671; b) H. Ness, A. J. Fisher, *Phys. Rev. B Condens. Matter* **1997**, *55*, 10081; c) M. I. J. Probert, A. J. Fisher, *J. Phys. Condens. Matter* **1997**, *9*, 3241; d) K. Schwarz, E. Nusterer, P. E. Blöchl, *Prepr. Am. Chem. Soc. Div. Pet. Chem.* **1997**, *42*, 69; e) N. A. W. Holzwarth, G. E. Matthews, R. B. Dunning, A. R. Tackett, Y. Zeng, *Phys. Rev. B Condens. Matter* **1997**, *55*, 2005; f) K. Schwarz, E. Nusterer, P. Margl, P. E. Blöchl, *Int. J. Quantum Chem.* **1997**, *61*, 369; g) M. I. J. Probert, A. J. Fisher, *Chem. Phys. Lett.* **1996**, *259*, 271; h) P. E. Blöchl, A. Togni, *Organometallics* **1996**, *15*, 4125; i) P. E. Blöchl, P. Margl, K. Schwarz, *ACS Symp. Ser.* **1997**, *629*, 54; j) P. Margl, T. Ziegler, P. E. Blöchl, *J. Am. Chem. Soc.* **1996**, *118*, 5412; k) C. Katan, P. E. Blöchl, P. Margl, C. Koenig, *Phys. Rev. B Condens. Matter* **1996**, *53*, 12112; l) E. Nusterer, P. Blöchl, K. Schwarz, *Chem. Phys. Lett.* **1996**, *253*, 448; m) P. Margl, J. C. W. Lohrenz, T. Ziegler, P. E. Blöchl, *J. Am. Chem. Soc.* **1996**, *118*, 4434; n) J. Sarnthein, K. Schwarz, P. E. Blöchl, *Phys. Rev. B: Condens. Matter* **1996**, *53*, 9084; o) P. Margl, T. Ziegler, P. E. Blöchl, *J. Am. Chem. Soc.* **1995**, *117*, 12625; p) P. Margl, K. Schwarz, P. E. Blöchl, *J. Chem. Phys.* **1995**, *103*, 683. q) P. Margl, K. Schwarz, P. E. Blöchl, *J. Chem. Phys.* **1994**, *100*, 8194. r) R. Nesper, K. Vogel, P. E. Blöchl, *Angew. Chem.* **1993**, *105*, 786 *Angew. Chem. Int. Ed. Engl* **1993,** *32*, 701.
[23] a) S. Nosè, *Mol. Phys.* **1984,** *52*, 255; b) W. G. Hoover, *Phys. Rev. A* **1985,** *31*, 1965.
[24] J. P. Perdew, A. Zunger, *Phys. Rev. B.* **1981**, *23*, 5048.
[25] D. Ceperley, B. J. Alder, *Phys. Rev. Lett.* **1980,** *45*, 566.
[26] A. D. Becke, *J. Chem. Phys.* **1992**, *96*, 2155.
[27] J. P. Perdew, *Phys. Rev. B.* **1986**, *33*, 8822.
[28] M. J. Frisch, G. W. Trucks, H. B. Schlegel, P. M. W. Gill, B. G. Johnson, M. A. Robb, J. R. Cheeseman, T. Keith, G. A. Petersson, J. A. Montgomery, K. Raghavachari, M. A. Al-Laham, V. G. Zakrzewski, J. V. Ortiz, J. B. Foresman, C. Y. Ayala, P. Y. Peng, W. Chen, M. W. Wong, J. L. Andres, E. S. Replogle, R. Martin, R. L. Gomperts, D. J. Fox, J. S. Binkley, D. J. Defrees, J. Baker, J. P. Stewart, M. Head-Gordon, C. Gonzales, J. A. Pople, *Gaussian 94*, *Rev. B.3*, Gaussian Inc., Pittsburgh PA, **1995**.
[29] G. Linhart, G. Dorffner, *VieNet2—Vienna Neural Network Toolkit 2*, Oesterreichisches Forschungsinstitut fuer Artificial Intelligence, TR-94-12, Wien, **1994**.
[30] The turning-points are defined by $|R(O_AH) - R(O_BH)| = \min.$, i.e., by the minimum difference between the O–H distances.
[31] The reaction coordinate is defined as $\rho = [R(O_AH) \times \cos\theta(O_BO_AH)]/R(OO)$, i.e., as the projection of the O_A–H distance onto the $O_A \cdots O_B$ connecting line, divided by the O–O distance.
[32] R. T. Skodje, *Annu. Rev. Phys. Chem.* **1993**, *44*, 145.